



## Research Article

# Studies of sintering temperature on the microstructure, magnetic and dielectric behavior of $\text{CaCu}_3\text{Ti}_{3.5}\text{Mn}_{0.5}\text{O}_{12}$ ceramic synthesized by semi-wet route

Santosh Pandey<sup>1</sup> · Vinod Kumar<sup>1</sup> · K. D. Mandal<sup>1</sup>

Received: 17 December 2019 / Accepted: 17 February 2020 / Published online: 24 February 2020  
© Springer Nature Switzerland AG 2020

## Abstract

The CCTMO ( $\text{CaCu}_3\text{Ti}_{3.5}\text{Mn}_{0.5}\text{O}_{12}$ ) ceramic has been prepared by using the semi-wet method and sintered at 1223 K, 1323 K, and 1373 K, respectively for 8 h. The XRD, as well as TEM, have been to confirm the phase formation of CCTMO ceramics. The crystalline size of CCTMO was found in the range of 38–70 nm at different sintering temperatures. The route-mean square, as well as average roughness, was occurred by AFM technique 7.55 nm and 9.23 nm, respectively, sintered at 1373 K. The P-E hysteresis loop shows the ferromagnetic behavior of CCTMO at room temperature for all samples. The zero-field cooled (ZFC), field cooled (FC) and Magnetic hysteresis (M-H) curve shows temperature-dependent ferromagnetic behavior of CCTMO ceramic. The dielectric constant ( $\epsilon_r$ ) at 10 kHz decreases with increasing sintering temperature due to semiconducting grains and insulating boundaries supported by internal barrier layer capacitance modal (IBLC) in Mn-doped CCTO ceramic.

**Keywords** Ceramic · Sintering temperature · Magnetic behavior · Dielectric property

## 1 Introduction

The  $\text{CaCu}_3\text{Ti}_4\text{O}_{12}$  (CCTO) has fascinated much importance due to the extraordinary perovskite structure and unexpected dielectrical behavior. The calcium copper titanate ceramic has been combined with 1:3 ratio A-site ordered perovskite  $\text{A}_1\text{Cu}_3\text{Ti}_4\text{O}_{12}$  with space group  $\text{Im}\bar{3}$ , combining the octahedral Ti-site of  $\text{TiO}_6$  and also combined with A-site of Cu square-planar [1, 2]. The CCTO ceramic type of perovskite containing giant dielectric constant with high tangent loss ( $\tan \delta$ ) and sensitivity of dielectric behaviors depend on the method of preparation [2]. Seriously, the major problem in the application of CCTO is a high tangent loss which urgently needs to develop a stable processing method. Till now, some theoretical method has been suggested to describe the origin of high dielectric constant and low dielectric loss ( $\tan \delta$ ) which finally assist to build up applications of CCTO perovskite material. These

methods are internal domain [3], electrode polarization effect [4], bimodal grain size model [5], internal barrier layer capacitance (IBLC) [6], and nanoscale barrier layer capacitance model (NBLC) [7]. The abnormal behavior of CCTO ceramic is most successfully described by the internal barrier layer capacitance (IBLC) model [8, 9]. This model suggests that *n*-type semiconducting grains are separated by insulating barriers corresponding to the Ti-rich secondary phase observed in grains boundaries [10, 11], creating a lot of insignificant capacitances and resulting in giant abnormal dielectric constant values. Afterward, the NBLC model also explained the behavior of dielectric constant on the basis of the existence of stacking faults by reconciling the opposing view of the intrinsic and extrinsic nature of Mn-doped CCTO ceramic [7]. Few of the occasions, dielectric loss, and non-linear permittivity were also explained by the different models and their results suggested that these are strongly associated with the microstructure of

✉ K. D. Mandal, kdmandal.apc@itbhu.ac.in | <sup>1</sup>Department of Chemistry, IIT (BHU), Varanasi, U.P 221005, India.



CCTO ceramic type of perovskite complexes which can be influenced by elemental doping and sintering condition [6, 12, 13]. The permittivity of CCTO ceramic was extremely depending on the preparation method, e.g., the dielectric function was also increased from  $10^3$  to  $10^4$  by varying the sintering temperature from 1273 to 1373 K [14]. Interestingly, during sintering, the dielectric constant was increased with the grain's growth and decrease with the resistance of grain boundaries [3, 5]. In the last decade, the CCTO perovskite-type of oxides achieved immense attention owing to their significance and potential impact in a ceramic capacitor, microwave device applications and other electronic devices [15]. CCTO was synthesized from the metal oxide at high temperature using a solid-state process. This method required long reaction time, high temperature calcination and sintering. Additionally, during synthesis some other secondary phases ( $\text{CuO}$ ,  $\text{TiO}_2$  and  $\text{Cu}_2\text{TiO}_3$ ) may also come out. On the other hand, synthesis by a process of a chemical solution such as sol–gel using metal alkoxide gives intimate and uniform atomic scale mixing of the metal ion. Titanium isopropoxide  $\text{Ti}(\text{OR})_4$  is very expensive at this route. So, we have synthesized the  $\text{CaCu}_3\text{Ti}_{3.5}\text{Mn}_{0.5}\text{O}_{12}$  ceramic via the semi-wet method and their relative studies of magnetic, dielectric properties and their microstructures of CCTMO sintered (for 8 h) at 1223 K, 1323 K, and 1373 K, respectively for 8 h [16]. This procedure possesses the benefit to upgrade dielectric function, tangent loss and magnetic behavior of  $\text{CaCu}_3\text{Ti}_{3.5}\text{Mn}_{0.5}\text{O}_{12}$  ceramic.

## 2 Experimental section

### 2.1 Materials and synthesis of $\text{CaCu}_3\text{Ti}_{3.5}\text{Mn}_{0.5}\text{O}_{12}$

The Mn-doped CCTO was prepared by the semi-wet method. Firstly in this technique, Mn-doped CCTO was synthesized through semi-wet route by using different analytical grade calcium nitrate,  $\text{Ca}(\text{NO}_3)_2 \cdot 4\text{H}_2\text{O}$  (98% Merck, India), Copper nitrate,  $\text{Cu}(\text{NO}_3)_2 \cdot 3\text{H}_2\text{O}$  (99% Merck, India), Manganese acetate,  $\text{Mn}(\text{CH}_3\text{COO})_2 \cdot 4\text{H}_2\text{O}$  (99% Merck, India), and titanium oxide,  $\text{TiO}_2$  (99% Merck, India), as a starting material in stoichiometric amount in molar ratio. The stoichiometric amount of  $\text{Ca}(\text{NO}_3)_2 \cdot 4\text{H}_2\text{O}$ ,  $\text{Cu}(\text{NO}_3)_2 \cdot 3\text{H}_2\text{O}$  and  $\text{Mn}(\text{CH}_3\text{COO})_2 \cdot 4\text{H}_2\text{O}$  were taken in double-distilled water. All the prepared solutions were mixed simultaneously in a beaker and the solid  $\text{TiO}_2$  was taken in the stoichiometric amount in the solution. The stoichiometric amount of citric acid (99.5%, Merck India) equivalent to metal ions was added in solution and mixed with each other. The resultant solution was heated on a hot plate magnetic stirrer at 243–248 K to evaporate water and allows for self-ignition. The ignition procedure occurred in

the air, which produced a grouping of gases and formed a fluffy mass of Mn-doped CCTO powders. Citric acid acts as a chelating agent that used as fuel which helps in the ignition step. The consequential Mn-doped CCTO was ground by using agate and mortar to form a fine powder. The CCTMO fine powder was calcined at 1073 K for 6 h. The calcined powder was used to create for cylindrical pellets with the use of 3% polyvinyl alcohol as a binder on applying 3 tons of pressure using hydraulic pressure for 120 s. Finally, the Mn-doped CCTO pellets (2 pallets) were sintered at 1223 K, 1323 K, and 1373 K, respectively for 8 h.

### 2.2 Characterization of $\text{CaCu}_3\text{Ti}_{3.5}\text{Mn}_{0.5}\text{O}_{12}$

The phase of Mn-doped CCTO perovskite sintered was recognized by an XRD (Rigaku mini flex 600, Japan) applying  $\text{Cu-K}_\alpha$  radiation (wavelength 1.5418 Å) with a scan rate of  $3^\circ/\text{min}$ . The morphology, as well as elemental composition, was examined by SEM (ZEISS; model EVO18 research, Germany) attached with an energy-dispersive X-ray analyzer (Oxford instrument, USA). The particle size was confirmed through a TEM (TEM, Technai G2 20 S-Twin). For TEM characterization, the sample was suspended in ethanol and sonicated 2 h. This suspension was dispersed on a carbon-coated copper grid and dried in oven 4 h. The thicknesses, as well as surface morphology, were analyzed using Atomic force microscopy (NTEGRA Prima, Germany). The magnetic behavior of Mn-doped CCTO was determined by Quantum Design MPMS-3, over a temperature range of 5 to 300 K at magnetic field  $\pm 2$  T. Temperature difference of zero-field cooled was determined at 100 Oe applied field were carried out using SQUID VSM dc magnetometer. The dielectric information of silver-coated cylindrical pellets was determined by LCR meter (PSM1735, NumetriQN<sub>4</sub>L, and U.K.).

## 3 Results and discussion

### 3.1 Microstructure analysis

The phase of  $\text{CaCu}_3\text{Ti}_{3.5}\text{Mn}_{0.5}\text{O}_{12}$  (CCTMO) ceramic powder confirmed by XRD sintered at 1223 K, 1323 K, and 1373 K, respectively for 8 h, depicts in Fig. 1. It shows the existence of CCTO as the main phase along with the slightly secondary phase of  $\text{TiO}_2$ . The diffraction patterns are exactly matched with JCPDS (card no.21-0140), which confirms the occurrence of the main phase formation of CCTO with the slight secondary phase with JCPDS (card no.46-1238) of  $\text{TiO}_2$  [17]. The crystalline size (D) of  $\text{CaCu}_3\text{Ti}_{3.5}\text{Mn}_{0.5}\text{O}_{12}$  was determined through the Debye Scherrer equation, which is shown below in Eq. (1).

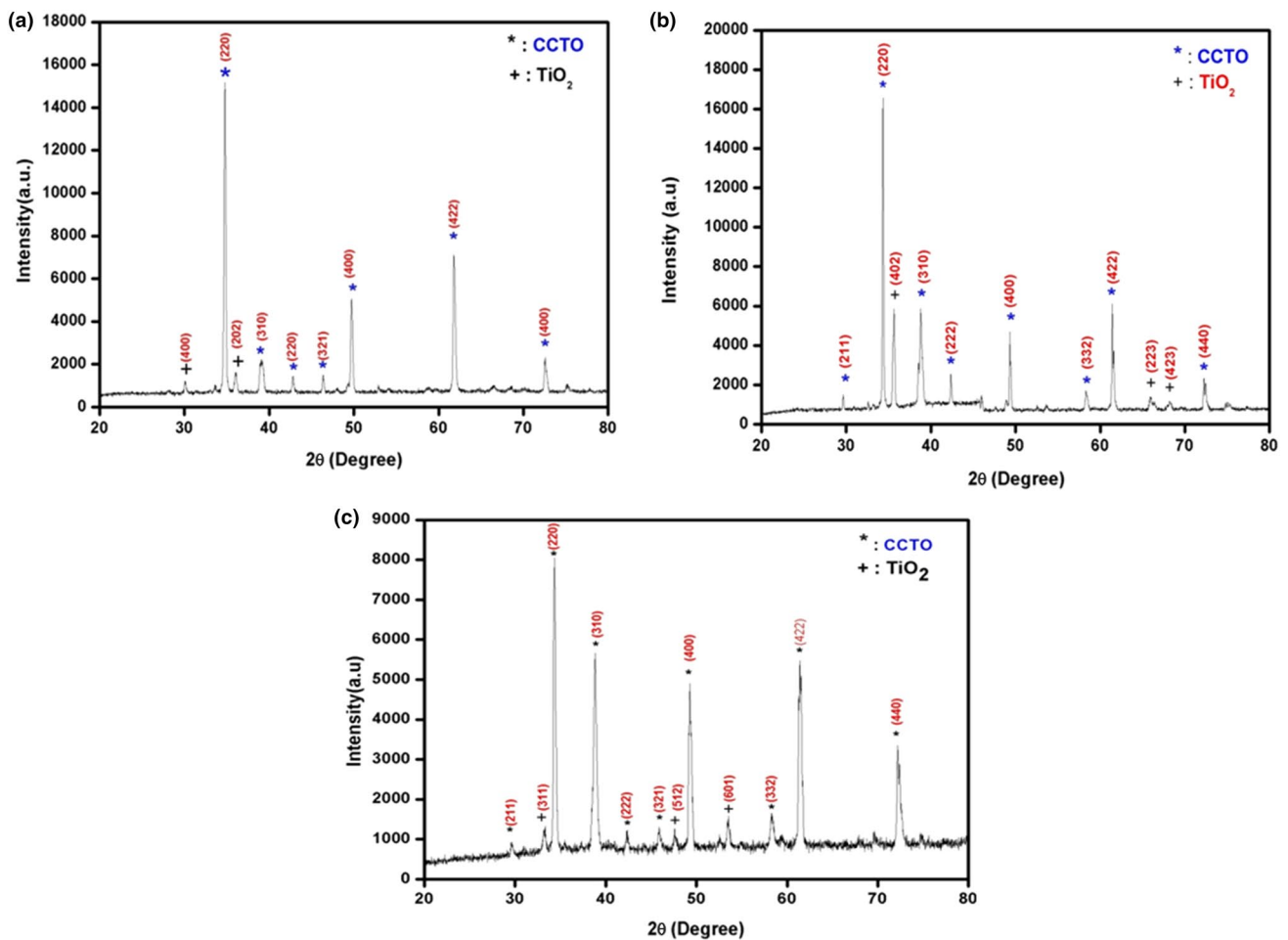


Fig. 1 XRD patterns of CCTMO sintered at **a** 1223 K **b** 1323 K **c** 1373 K for 8 h

$$D = \frac{K\lambda}{\beta \cos\theta} \quad (1)$$

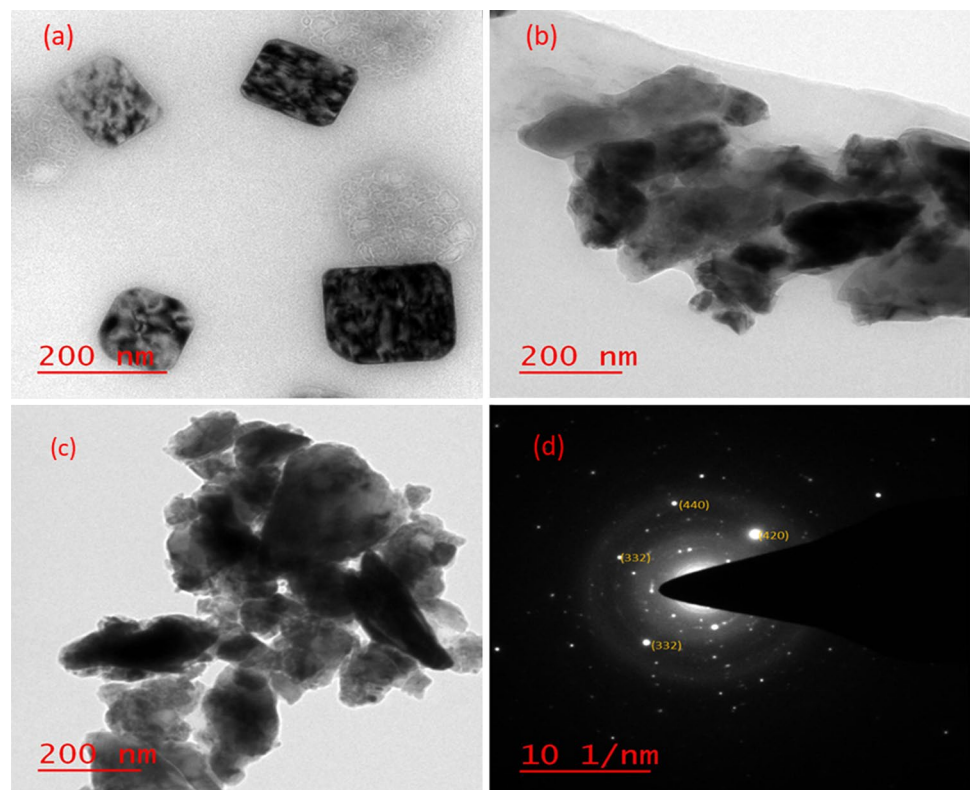
where  $D$  is crystallite size,  $k$  is constant equal to 0.89,  $\lambda$  is a wavelength of X-ray,  $\theta$  is the Bragg diffraction angle and  $\beta$  is the full width at half maximum (FWHM) in radians. For the determination of the accurate value of crystalline size, the line broadening due to instrumental effect removed by adding a standard sample for XRD data. The average crystallite size of  $\text{CaCu}_3\text{Ti}_{3.5}\text{Mn}_{0.5}\text{O}_{12}$  was calculated  $38.97 \pm 10$  nm,  $69.32 \pm 10$  nm and  $36.54 \pm 10$  nm at 1223 K, 1323 K, and 1373 K, for 8 h, respectively.

Figure 2a–c presents the bright-field TEM images of  $\text{CaCu}_3\text{Ti}_{3.5}\text{Mn}_{0.5}\text{O}_{12}$  (CCTMO) sintered at 1223 K, 1323 K, and 1373 K, respectively for 8 h. The particle size of CCTMO calculated by TEM is found to be  $98.49 \pm 10$  nm,  $92.95 \pm 10$  nm and  $145.50 \pm 10$  nm at 1223 K, 1323 K and 1373 K, respectively. It is found that the particle size depends on sintering temperature and the sintering temperature increases as particle size. The particle

size and average crystalline size are closed with each other determined by TEM as well as XRD. The selected area diffraction pattern (SEAD) is also shown in Fig. 2d of  $\text{CaCu}_3\text{Ti}_{3.5}\text{Mn}_{0.5}\text{O}_{12}$  ceramic sintered at 1373 K which was confirmed the existence of single-phase nanocrystalline material. The diffraction pattern was indexed according to a cubic crystal structure and calculated lattice parameter was found to be 7.393 Å. The lattice parameter observed from the SEAD pattern was in good agreement with value obtained from the JCPDS card no. 21-0140 for XRD data.

Figure 3a–c shows the SEM micrograph of  $\text{CaCu}_3\text{Ti}_{3.5}\text{Mn}_{0.5}\text{O}_{12}$  ceramic sample sintered at 1223 K, 1323 K, and 1373 K, respectively for 8 h. The substituting of Mn in  $\text{CaCu}_3\text{Ti}_4\text{O}_{12}$  significantly affects the surface morphology [18]. The grain size of  $\text{CaCu}_3\text{Ti}_{3.5}\text{Mn}_{0.5}\text{O}_{12}$  ceramic at low temperature i.e. 1223 K shows large-grained with grain size 1.05  $\mu\text{m}$ . The grain size of  $\text{CaCu}_3\text{Ti}_{3.5}\text{Mn}_{0.5}\text{O}_{12}$  ceramic at high temperature i.e. 1323 K as well as 1373 K is about 9.50  $\mu\text{m}$  and 14.87  $\mu\text{m}$ , respectively. The grain size regularly increases with respect to temperature. In general,

**Fig. 2** Bright-field TEM images at **a** 1223 K **b** 1323 K **c** 1373 K and **d** Selected area diffraction pattern of CCTMO at 1373 K



at low-temperature grain boundaries are not clear but at high-temperature grains and grain boundary, both are clearly visible in Fig. 3b, c. The increase the grain size with respect to the temperature of CCTMO ceramic may be due to enlarged grain boundary mobility. Figure 3d–f shows the EDX spectra of Mn-doped CCTO ceramic sintered at 1223 K, 1323 K and 1373 K, respectively for 8 h [11], which verify the existence of Ca, Cu, Mn, Ti, and O elements. The weight percentage of Ca, Cu, Mn, Ti, and O elements is presented in Table 1 with different temperatures were confirmed the stoichiometry and purity of the materials.

Figure 4a presents 2-D Atomic Force Micrograph (AFM) of  $\text{CaCu}_3\text{Ti}_{3.5}\text{Mn}_{0.5}\text{O}_{12}$  ceramic sintered at 1373 K for 8 h, which shows cubical structures of grain separate by a grain boundary. The average roughness ( $R_a$ ), as well as root mean square roughness ( $R_q$ ) was obtained as 7.55 nm and 9.23 nm, respectively on a scanned area  $5.0 \mu\text{m} \times 5.0 \mu\text{m}$ . Figure 4b depicts the distribution of particle on the surface which was observed in the 3-D structure. The grain size determined by the histogram graph occurs in the range of 0.8–1.5  $\mu\text{m}$  and the average particle size was found to be 0.44  $\mu\text{m}$  out of the 514 grains shown in Fig. 4c.

Figure 5 illustrates the main Mn 2p XPS range for CCTMO samples sintered at 1223 K for 8 h. The highest peak is shown in Fig. 5 at 642.8, 649 and 652 eV as against Mn 2p<sub>3/2</sub> and Mn 2p<sub>1/2</sub>, respectively. According to the spin–spin orbital coupling, the splitting of peak Mn 2p into

Mn 2p<sub>3/2</sub> and Mn 2p<sub>1/2</sub> takes place. The shoulder occurred at higher energy is shown along the width of the peak for Mn 2p<sub>3/2</sub> and Mn 2p<sub>1/2</sub> as shown by arrows, indicating contributions from the mixed valent state of Mn ions is present. Because of this, Mn 2p<sub>3/2</sub> and Mn 2p<sub>1/2</sub> can each divide further into two other peaks. The Mn 3p<sub>3/2</sub> deconvoluted peak at 640.12 eV and 641.6 eV (Mn 2p<sub>1/2</sub> at 653 and 655 eV) represents both the Mn<sup>3+</sup> and the Mn<sup>4+</sup>, respectively. This data confirms the Mn present in both +3 and +4 oxidation state [19]

### 3.2 Magnetic studies

In order to prove the magnetization behavior of Mn-doped CCTO ceramic sintered 1373 K for h, the temperature dependence of ZFC and FC magnetization was recorded in a temperature range of 5–300 K with 100 Oe as an applied field shown in Fig. 6a. The transitions show between ZFC and FC just about at 114 K. The magnetization increases quickly in the FC curve that proves the existence of ferromagnetic behavior of CCTMO ceramic. Meanwhile, in CCTMO ceramic only one critical temperature is detecting around 114 K [20]. However, CCTMO ceramic ZFC and FC curve decrease with increasing temperature. The M-H hysteresis curves measured at two different temperatures (5, 300 K) and applied field  $\pm 2$  T for  $\text{CaCu}_3\text{Ti}_{3.5}\text{Mn}_{0.5}\text{O}_{12}$  is depicted in Fig. 6b. The M-H hysteresis curves display a



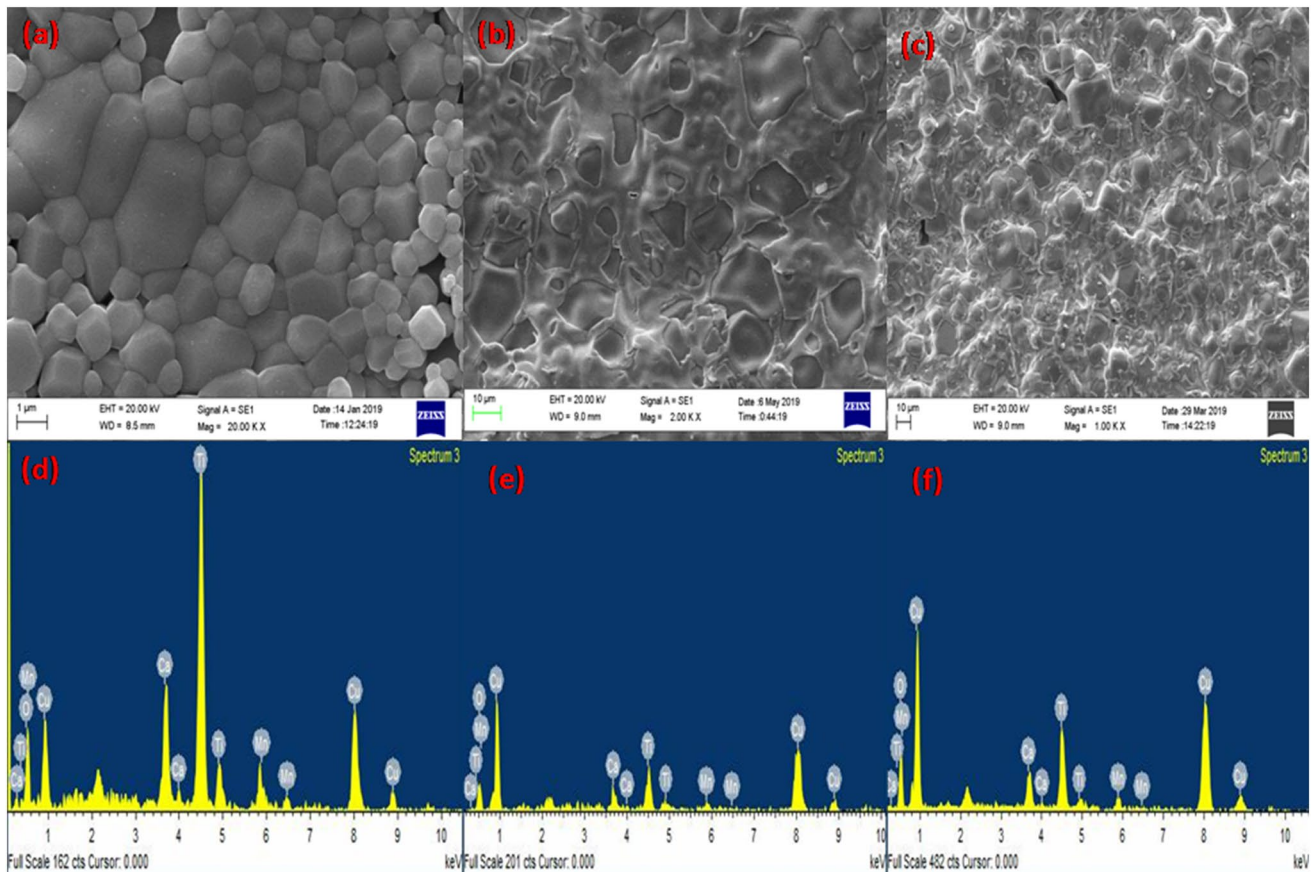


**Fig. 3** a–c SEM micrograph and d–e EDX spectra of CCTMO ceramic sintered at 1223 K, 1323 K, and 1373 K, respectively for 8 h

**Table 1** Weight percentage of elements for  $\text{CaCu}_3\text{Ti}_{3.5}\text{Mn}_{0.5}\text{O}_{12}$  sintered at 1223 K, 1323 K and 1373 K, respectively for 8 h

Temperature (K)	Weight percent of elements				
	Ca (%)	Cu (%)	Ti (%)	Mn (%)	O (%)
1223	6.60	29.67	28.81	4.12	30.80
1323	3.54	64.24	10.68	2.76	18.78
1373	3.80	58.12	11.65	2.58	23.56

linear behavior similar to the anti-ferromagnetic system at 5 K due increased moment. Further, the linear behavior in the magnetic moment along with the magnetic field is recorded with an increase of temperature (300 K) which confirms the existence of paramagnetic behavior of the material [21]. Figure 7 describes the temperature-dependent reciprocal of magnetic susceptibility for  $\text{CaCu}_3\text{Ti}_{3.5}\text{Mn}_{0.5}\text{O}_{12}$  ceramic. The Weiss temperature ( $\theta$ ) and Curie constant ( $C$ ) can be determined by using the Curie–Weiss law, represented by the following equation.

$$\chi = \frac{C}{T - \theta} \tag{2}$$

where  $\chi$  is magnetic susceptibility,  $C$  is curie constant,  $\theta$  is Curie Weiss temperature and  $T$  is temperature. The calculated value of Curie constant ( $C$ ) and Weiss temperature ( $\theta$ ) obtained by this plot was found to be  $5811.76 \text{ emus/g}^{-1}$  and  $57.04 \text{ K}$ , respectively. The positive value of  $\theta$  confirms the ferromagnetic behavior of Mn-doped CCTO ceramic.

Figure 8 depicts the polarization against the electric field P-E hysteresis loop of  $\text{CaCu}_3\text{Ti}_{3.5}\text{Mn}_{0.5}\text{O}_{12}$  ceramic was detected at room temperature (308 K). This estimation was carried out at a frequency of 150 Hz. As the increasing temperature, the nature of the loop has been changed to become slimmer. This type of behavior of the P-E loop represents the evolution process of relaxor ferroelectrics [22]. By applying the electric field resultant remnant polarization ( $P_r$ ) increases with increasing sintering temperature of  $\text{CaCu}_3\text{Ti}_{3.5}\text{Mn}_{0.5}\text{O}_{12}$  materials. The measured remnant polarization ( $P_r$ ) of CCTMO ceramic is  $0.827, 0.989$  and  $1.005 \mu\text{C/cm}^2$  at 1223 K, 1323 K and 1373 K, respectively. On the applying, high electric field saturation has not occurred in the P-E loop which might be due to the combined effect of capacitor and resistor joint in parallel (lossy capacitor) of these materials [23].

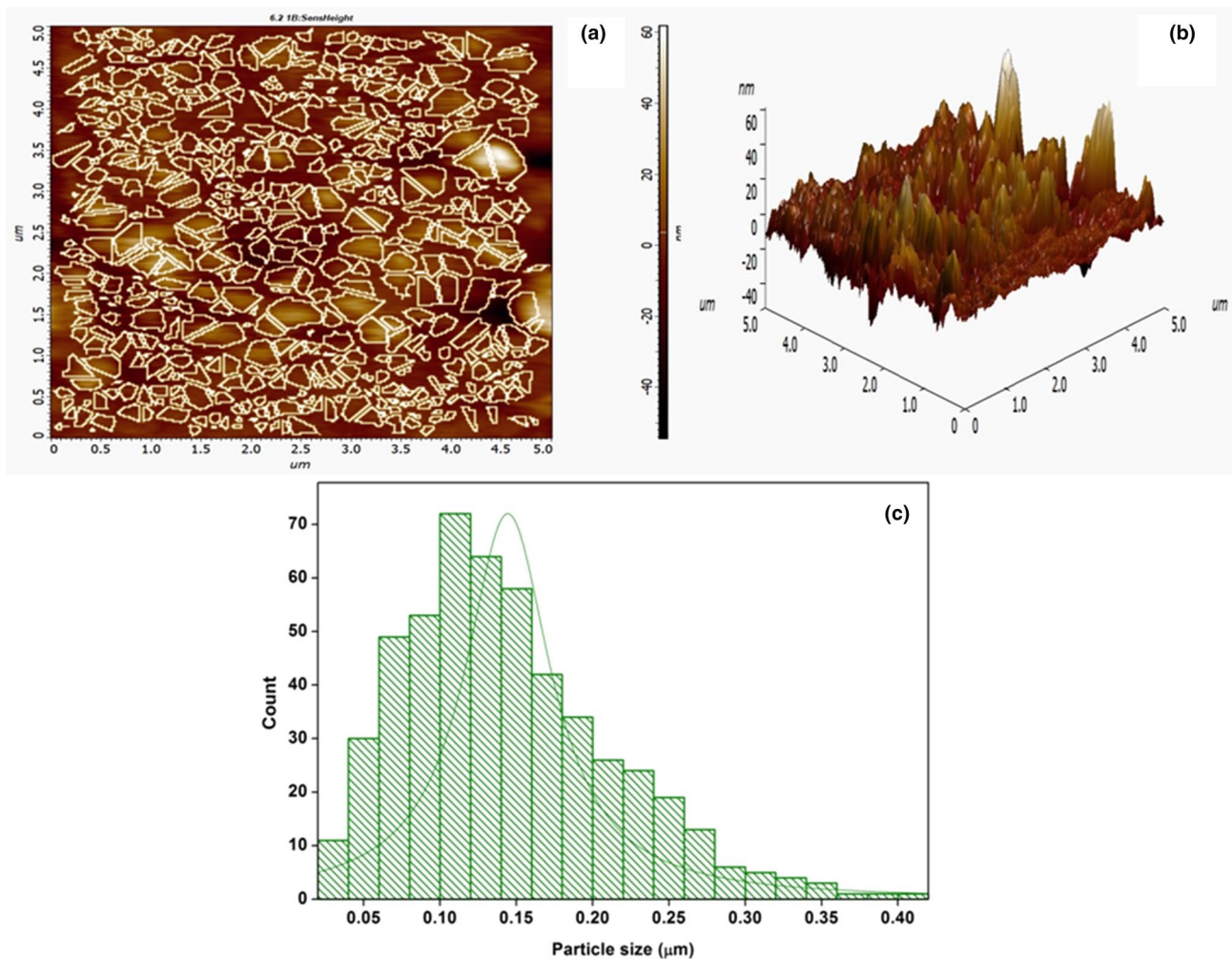


**Fig. 4** AFM images of CCTMO ceramics sintered at 1373 K for 8 h **a** 2-dimensional structure **b** 3-dimensional structure **c** bar diagram of particle size

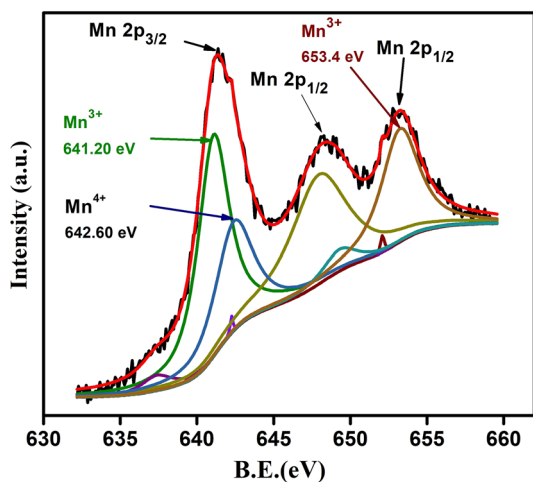


**Fig. 5** X-ray photo emission spectroscopy of Mn 2p, sintered at 1223 K for 8 h

### 3.3 Dielectric studies

Figure 9 depicts the results of temperature-dependent dielectric function ( $\epsilon_r$ ) and tangent loss ( $\tan \delta$ ) at 10 kHz for sintered 1223 K, 1323 K, and 1373 K, respectively for 8 h. The data specify that the  $\text{CaCu}_3\text{Ti}_{3.5}\text{Mn}_{0.5}\text{O}_{12}$  ceramic depicts an important effect on the dielectric behavior at 35 °C (r t). The variation in dielectric function ( $\epsilon_r$ ) can be assigned to the differences in the grain size distribution. Mn-doped CCTO ceramic has a lower permittivity ( $\epsilon_r$ ) than pure CCTO ceramic sample [24]. The dielectric function of pure CCTO indicates the giant value around 20,000 at 300 K, but the value of dielectric function decreases abruptly with a decreasing temperature below 120 K [25]. The dielectric function increases with increasing temperature due to the capability of the charge carriers to an alien with applied field increases at higher temperatures [24]. However, we observed that the value of

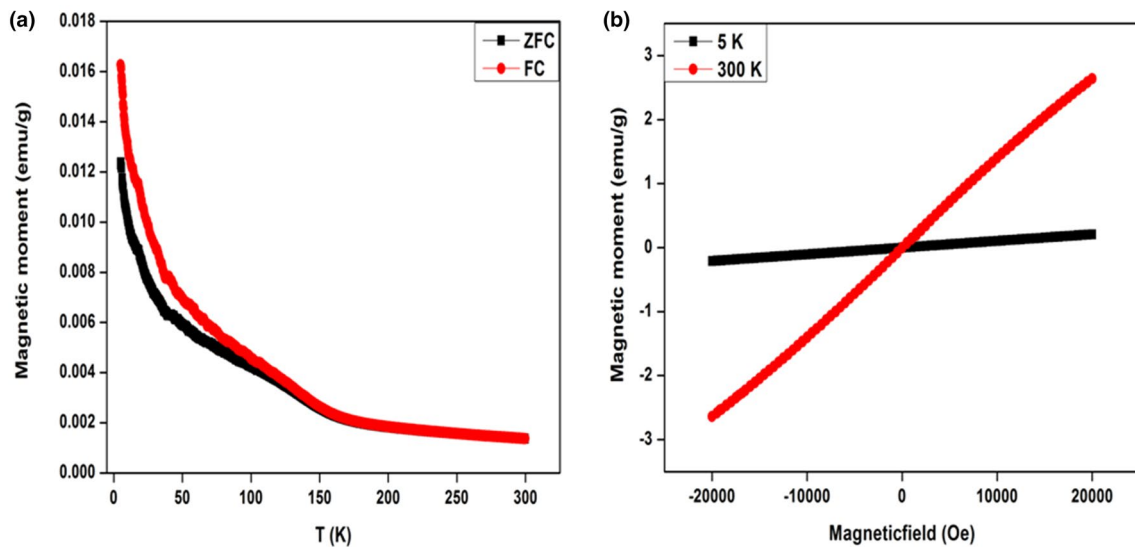


**Fig. 6** Temperature-dependent **a** magnetic moment noted applied magnetic field at 100 Oe. **b** M-H hysteresis at 5 and 300 K for CCTMO ceramic sintered at 1323 K for 8 h

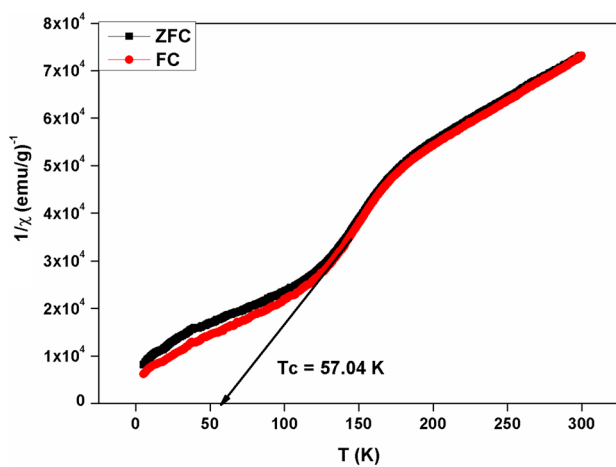


**Fig. 7** Magnetic susceptibility as a function of temperature recorded at  $\pm 2$  T and applied magnetic field (H) at 100 Oe

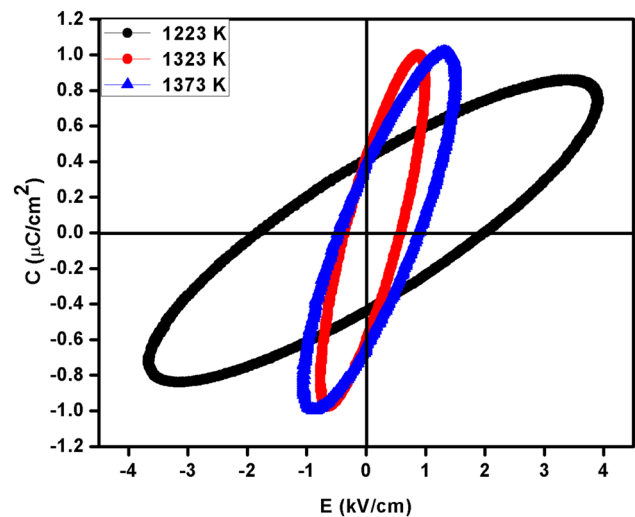
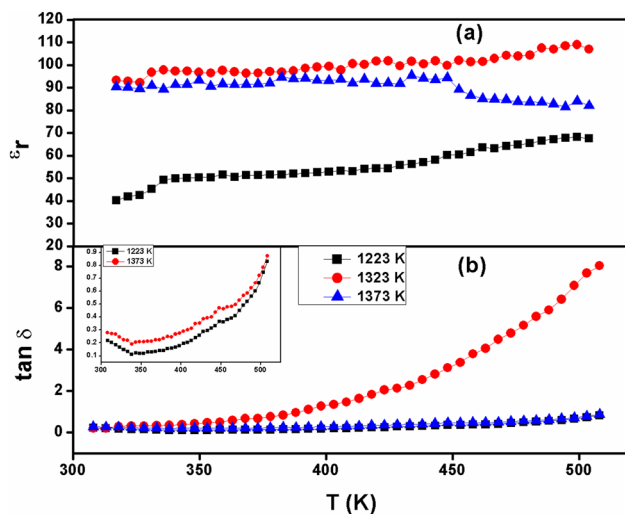


**Fig. 8** The polarization versus electric field (P-E) hysteresis loop of  $\text{CaCu}_3\text{Ti}_{3.5}\text{Mn}_{0.5}\text{O}_{12}$  at sintered at 1223 K, 1323 K, and 1373 K, respectively

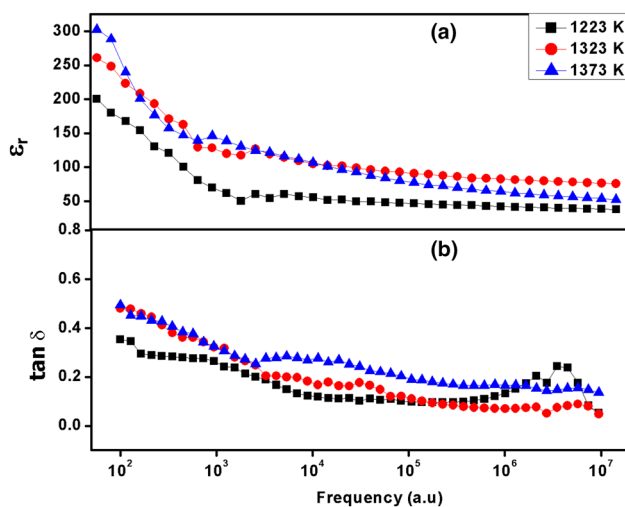
the dielectric function of CCTMO decreases from 25,000 to 100 at 300 K (R.T) shows in Fig. 9a. This result is clearly confirmed that little quantity of Mn-doping on the Ti-sites in CCTO produced an astonishing effect on dielectric behaviors of CCTMO ceramic. In Fig. 9a we found that the value of dielectric function increases with rising sintering temperature [26]. The values of dielectric function are found to be 40, 90 and 95 at 10 kHz for sintering temperature at 1223 K, 1323 K and 1373 K, respectively for 8 h. The tangent loss ( $\tan \delta$ ) increases slightly from 300 to 380 K, and thereafter rises quickly with rising temperature to 508 K for all sintering temperatures shows in

Fig. 9b. The value of tangent loss ( $\tan \delta$ ) was obtained to be less than 0.3 at 10 kHz for all sintering temperatures.

Figure 10 presents the frequency-dependent dielectric function ( $\epsilon_r$ ) and tangent loss ( $\tan \delta$ ) at room temperature for sintered at 1223 K, 1323 K, and 1373 K, respectively for 8 h. The value of the dielectric function ( $\epsilon_r$ ) is found to be 200, 260 and 00 at sintering temperature 1223 K, 1323 K and 1373 K, respectively shows in Fig. 10a. However, the Mn-doping decreases dielectric constant ( $\epsilon_r$ ) and in fact refine the tangent loss ( $\tan \delta$ ) at room temperature at around medium frequency region. The tangent loss ( $\tan$



**Fig. 9** Temperature-dependent **a** dielectric constant ( $\epsilon_r$ ) and **b** loss tangent ( $\tan \delta$ ) at 10 kHz for sintered at 1223 K, 1323 K, and 1373 K, respectively for 8 h



**Fig. 10** Frequency-dependent **a** dielectric constant ( $\epsilon_r$ ) and **b** loss tangent ( $\tan \delta$ ) at room temperature for sintered at 1223 K, 1323 K, and 1373 K, respectively

$\delta$ ) is found to be less than 0.5 for all sintering temperature shows in Fig. 10b.

## 4 Conclusions

The Mn-doped calcium copper titanium oxide;  $\text{CaCu}_3\text{Ti}_4\text{O}_{12}$  was prepared by the semi-wet route. The phase of CCTMO was detected by XRD and crystallite size obtained from the XRD data were occurred to be  $38.97 \pm 10$  nm,  $69.32 \pm 10$  nm and  $36.54 \pm 10$  nm at 1223 K, 1323 K, and 1373 K, for 8 h, respectively. The particle size obtained by

TEM is  $98.49 \pm 10$  nm,  $92.95 \pm 10$  nm and  $145.50 \pm 10$  nm at 1223 K, 1323 K and 1373 K, respectively. The EDX spectra confirmed the presence of Ca, Cu, Ti, Mn, O element in  $\text{CaCu}_3\text{Ti}_{3.5}\text{Mn}_{0.5}\text{O}_{12}$  ceramic in stoichiometric ratio as the molecular formula. The dielectric function ( $\epsilon_r$ ) and tangent loss were occurred to be 40–300 and 0.2–0.6 at room temperature. The dielectric function increases and tangent loss decreases with increasing sintering temperature.

**Acknowledgements** The author would like to show gratitude in-charge of CIFIC, IIT (BHU) Varanasi for SEM, TEM, AFM and MPMS facilities. the authors Santosh Pandey is thankful to IIT (BHU) (Grant no.17051002) for financial support for teaching assistantship.

## Compliance with ethical statement

**Conflict of interest** The authors declare that they have no conflict of interest.

## References

- Subramanian MA, Sleight AW (2002)  $\text{ACu}_3\text{Ti}_4\text{O}_{12}$  and  $\text{ACu}_3\text{Ru}_4\text{O}_{12}$  perovskites: high dielectric constants and valence degeneracy. *Solid State Sci* 4:347–351
- Schmidt R, Stennett MC, Hyatt NC, Pokorný J, Prado-Gonjal J, Li M, Sinclair DC (2012) Effects of sintering temperature on the internal barrier layer capacitor (IBLC) structure in  $\text{CaCu}_3\text{Ti}_4\text{O}_{12}$  (CCTO) ceramics. *J Eur Ceram Soc* 32:3313–3323
- Fang TT, Liu CP (2005) Evidence of the internal domains for inducing the anomalously high dielectric constant of  $\text{CaCu}_3\text{Ti}_4\text{O}_{12}$ . *Chem Mater* 17:5167–5171
- Lunkenheimer P, Fichtl R, Ebbinghaus SG, Loidl A (2004) Non-intrinsic origin of the colossal dielectric constants in  $\text{CaCu}_3\text{Ti}_4\text{O}_{12}$ . *Phys Rev B* 70:172102
- Pan MJ, Bender BA (2005) A bimodal grain size model for predicting the dielectric constant of calcium copper titanate ceramics. *J Am Ceram Soc* 88:2611–2614
- Senda S, Rhouma S, Torkani E, Megriche A, Autret C (2005) Effect of nickel substitution on electrical and microstructural properties of  $\text{CaCu}_3\text{Ti}_4\text{O}_{12}$  ceramic. *J Alloys Compd* 698:152–158
- Bueno PR, Tararan R, Parra R, Joanni E, Ramírez MA, Ribeiro WC, Longo E, Varela JA (2009) A polaronic stacking fault defect model for  $\text{CaCu}_3\text{Ti}_4\text{O}_{12}$  material: an approach for the origin of the huge dielectric constant and semiconducting coexistent features. *J Phys D Appl Phys* 42:055404
- Fiorenza P, Lo R, Nigro C, Bongiorno V, Raineri MC, Ferarrelli DC, Sinclair ARW (2008) Localized electrical characterization of the giant permittivity effect in  $\text{CaCu}_3\text{Ti}_4\text{O}_{12}$  ceramics. *Appl Phys Lett* 92:182907
- Singh L, Rai US, Mandal KD (2013) Dielectric, modulus and impedance spectroscopic studies of nanostructured  $\text{CaCu}_{2.70}\text{Mg}_{0.30}\text{Ti}_4\text{O}_{12}$  electro-ceramic synthesized by modified sol-gel route. *J Alloys compd* 555:176–183
- Fernandez JF, Leret P, Romero JJ, De J, Frutos J, De La Rubia MA, Martín González MS, Costa-Krämer JL, Fierro JL, Quesada A, García MA (2009) Proofs of the coexistence of two magnetic contributions in pure and doped  $\text{CaCu}_3\text{Ti}_4\text{O}_{12}$  giant dielectric constant ceramics. *J Am Ceram Soc* 92:2311–2318
- Pandey S, Mandal KD (2019) Investigation of microstructure, ferroelectric and dielectric behavior of  $\text{CaCu}_3\text{Ti}_{(4-x)}\text{Mn}_x\text{O}_{12}$  perovskites synthesized through semi-wet route. *Sn Appl Sci* 1:1738



12. Li T, Chen J, Liu D, Zhang Z, Chen Z, Li Z, Cao X, Wang B (2014) Effect of NiO-doping on the microstructure and the dielectric properties of  $\text{CaCu}_3\text{Ti}_4\text{O}_{12}$  ceramics. *Ceram Int* 40:9061–9067
13. Zheng Q, Fan H, Long C (2012) Microstructures and electrical responses of pure and chromium-doped  $\text{CaCu}_3\text{Ti}_4\text{O}_{12}$  ceramics. *J Alloys Compd* 511:90–94
14. Bender BA, Pan MJ (2005) The effect of processing on the giant dielectric properties of  $\text{CaCu}_3\text{Ti}_4\text{O}_{12}$ . *Mater Sci Eng B* 117:339–347
15. Shay DP, Podraza NJ, Donnelly NJ, Randall CA (2012) High energy density, high temperature capacitors utilizing Mn-doped  $0.8\text{CaTiO}_3-0.2\text{CaHfO}_3$  ceramics. *J Am Ceram Soc* 95:1348–1355
16. Pandey S, Kumar A, Singh NB, Mandal KD (2019) Studies on dielectric and magnetic properties of  $\text{CaCu}_3\text{Ti}_3\text{MnO}_{12}$  ceramic synthesized via semi-wet route. *J Aust Ceram Soc* 2019:1–8
17. Cai J, Lin YH, Cheng B, Nan CW, He J, Wu Y, Chen X (2007) Dielectric and nonlinear electrical behaviours observed in Mn-doped  $\text{CaCu}_3\text{Ti}_4\text{O}_{12}$  ceramic. *Appl Phys Lett* 91:252905
18. Xu Z, Qiang H (2017) Enhanced dielectric properties of Zn and Mn Co-doped  $\text{CaCu}_3\text{Ti}_4\text{O}_{12}$  ceramics. *J Mater Sci Mater El* 28:376–380
19. Jaiswar S, Mandal KD (2017) Evidence of enhanced oxygen vacancy defects inducing ferromagnetism in multiferroic  $\text{CaMn}_7\text{O}_{12}$  manganite with sintering time. *J Phys Chem C* 1121:19586–19601
20. Han D, Wu Z, Wang Z, Yang S (2016) Oriented Mn-doped CuO nanowire arrays. *Nanotechnology* 27:135603
21. Pal K, Dey A, Ray PP, Mordvinova NE, Lebedev OI, Mandal TK, Seikh MM, Gayen A (2018) Synthesis, characterization and catalytic activity of quadruple perovskite:  $\text{CaCu}_{3-x}\text{Mn}_x\text{Ti}_{4-x}\text{Mn}_x\text{O}_{12}$  ( $x=0, 0.5$  and  $1.0$ ). *Chem Sel* 3:1076–1087
22. Huang CJ, Li K, Wu SY, Zhu XL, Chen XM (2015) Variation of ferroelectric hysteresis loop with temperature in  $(\text{Sr}_x\text{Ba}_{1-x})\text{Nb}_2\text{O}_6$  unfilled tungsten bronze ceramics. *J Materiomics* 1:146–152
23. Stewart MG, Cain MG, Hall DA (1999) Ferroelectric hysteresis measurement and analysis. National Physical Laboratory, Teddington
24. Z. Xu, H. Qiang 2017 Enhanced dielectric properties of Zn and Mn co-doped  $\text{CaCu}_3\text{Ti}_4\text{O}_{12}$  ceramics. *J Mater Sci-Mater El*. 28:376–80
25. Chung SY, Kim ID, Kang SJ (2004) Strong nonlinear current–voltage behaviour in perovskite-derivative calcium copper titanate. *Nat Mater* 3:774
26. Krohns S, Lunkenheimer P, Ebbinghaus SG, Loidl A (2008) Colossal dielectric constants in single-crystalline and ceramic  $\text{CaCu}_3\text{Ti}_4\text{O}_{12}$  investigated by broadband dielectric spectroscopy. *J Appl Phys* 103:084107

**Publisher's Note** Springer Nature remains neutral with regard to jurisdictional claims in published maps and institutional affiliations.